PALEOCEANOGRAPHY, VOL. 28, 283–295, doi:10.1002/palo.20028, 2013

Atlantic Water advection versus sea-ice advances in the eastern Fram Strait during the last 9 ka: Multiproxy evidence for a two-phase Holocene

Kirstin Werner,[1] Robert F. Spielhagen,[1,2] Dorothea Bauch,[1,2] H. Christian Hass,[3] and Evgeniya Kandiano[1]

Received 18 September 2012; revised 28 January 2013; accepted 25 March 2013; published 31 May 2013.

[1] A sediment core from the West Spitsbergen continental margin was studied to reconstruct climate and paleoceanographic variability during the last ~9 ka in the eastern Fram Strait (FS). Our multiproxy evidence suggests that the establishment of the modern oceanographic configuration in the eastern FS occurred stepwise, in response to the postglacial sea-level rise and the related onset of modern sea-ice production on the shallow Siberian shelves. The late Early and Mid-Holocene interval (9 to 5 ka) was generally characterized by relatively unstable conditions. High abundance of the subpolar planktic foraminifer species *Turborotalita quinqueloba* implies strong intensity of Atlantic Water (AW) inflow with high productivity and/or high AW temperatures, resulting in a strong heat flux to the Arctic. A series of short-lived cooling events (8.2, 6.9, and 6.1 ka) occurred superimposed on the warm late Early to Mid-Holocene conditions. Our proxy data imply that simultaneous to the complete postglacial flooding of Arctic shallow shelves and the initiation of modern sea-ice production, strong advance of polar waters initiated modern oceanographic conditions in the eastern FS at ~5.2 ka. The Late Holocene was marked by the dominance of the polar planktic foraminifer species *Neogloboquadrina pachyderma*, a significant expansion of sea ice/icebergs, and strong stratification of the water column. Although planktic foraminiferal assemblages as well as sea subsurface temperatures suggest a return of slightly strengthened advection of subsurface AW after 3 ka, a relatively stable cold-water layer prevailed at the sea surface, and the study site was probably located within the seasonally fluctuating marginal ice zone during the Neoglacial period.

Citation: Werner, K., R. F. Spielhagen, D. Bauch, H. C. Hass, and E. Kandiano (2013), Atlantic Water advection versus sea-ice advances in the eastern Fram Strait during the last 9 ka: Multiproxy evidence for a two-phase Holocene, *Paleoceanography*, *28*, 283–295, doi:10.1002/palo.20028.

1. Introduction

[2] The Arctic Ocean is sensitive to global atmospheric and oceanographic changes [*Moritz et al*., 2002; *Serreze and Francis*, 2006]. Sea-ice loss and its consequences, such as lowering the albedo and enhancing the heat transport from the ocean to the atmosphere, amplify the effect of climate change [*Manabe and Stouffer*, 1980; *Serreze et al*., 2007]. Climate variations during the Early and Mid-Holocene are an adequate reference for recent climate excursions such as the ongoing global warming and the Little Ice Age period. The temperature rise within the last 100 to 150 years has been noted in both terrestrial and marine high-resolution proxy records from the northern hemisphere [*Overpeck et al*, 1997; *Moberg et al*., 2005; *Kaufman et al*., 2009; *Mann et al*., 2009; *Spielhagen et al*., 2011].

[3] The eastern Fram Strait (FS) is the main gateway where warm, saline Atlantic Water (AW) enters the Arctic Ocean, and heat exchange through FS is crucial for Arctic Ocean temperatures and sea-ice extent [*Karcher et al*., 2003; *Schauer et al*., 2004]. An increasing number of studies from the Barents Sea/Svalbard area [e.g., *Sarnthein et al*., 2003; *Hald et al*., 2004, 2007; *Ślubowska et al*., 2005; *Rasmussen et al*., 2007; *Ślubowska-Woldengen et al*., 2007, 2008; *Jessen et al*., 2010; *Risebrobakken et al*., 2010, 2011] and the Nordic Seas [e.g., *Koç et al*., 1993; *Bauch et al*., 2001a; *Risebrobakken et al*., 2003] report significant variations in temperature and current strength of surface and deep water during the past 10,000 years. Studies of marine sediment cores around Svalbard agree on thermal maximum conditions during the Early Holocene commencing ~10 cal ka BP [e.g., *Hald et al*., 2004, 2007; *Ślubowska et al*., 2005; *Ebbesen et al*., 2007; *Rasmussen et al*., 2007;

[1]Helmholtz Centre for Ocean Research Kiel GEOMAR, Kiel, Germany.
[2]Academy of Sciences, Humanities, and Literature Mainz, Mainz, Germany.
[3]Alfred Wegener Institute for Polar and Marine Research, Wadden Sea Station Sylt, List/Sylt, Germany.

Corresponding author: K. Werner, Helmholtz Centre for Ocean Research Kiel GEOMAR, Wischhofstraße 1–3, DE-24148 Kiel, Germany. (kwerner@geomar.de)

0883-8305/13/10.1002/palo.20028

Ślubowska-Woldengen et al., 2007, 2008] but show some inconsistencies for the development of the Mid- and Late Holocene. There is a general agreement on a cooling trend after ~8 cal ka BP [*Hald et al*., 2004; *Ślubowska-Woldengen et al*., 2007], though some records indicate a relatively warm Mid-Holocene in the Barents Sea/Svalbard area with temperatures higher than for the remainder of the Holocene [e.g., *Sarnthein et al*., 2003]. However, these Mid-Holocene temperatures were still not as high as those of the Early Holocene [e.g., *Hald et al*., 2007; *Rasmussen et al*., 2007].

[4] The most pronounced climate excursion of the Holocene period found in Greenland ice core data is the so-called "8.2 ka cooling event" [*Stuiver et al*., 1995] which was likely triggered by the final outburst drainage from the glacial lakes Agassiz/Ojibway during the final collapse of the Laurentide Ice Sheet (LIS) [*Barber et al*., 1999]. The corresponding immense meltwater release into the North Atlantic [e.g., *Stuiver et al*., 1995; *Rohling and Pälike*, 2005] resulted in a short-lived cool, dry, and possibly windy climate event [*Alley et al*., 1997]. Strong short-term climate fluctuations between ~8.4 and 8.0 cal ka BP are well pronounced in many records of the North Atlantic [*Alley et al*., 1997; *Risebrobakken et al*., 2003; *Hall et al*., 2004; *Moros et al*., 2004; *Hald et al*., 2007; *Kleiven et al*., 2008]. Other studies reveal longer-lasting cool intervals between 8.8 and 8.0 cal ka BP [e.g., *Sarnthein et al*., 2003; *Keigwin et al*., 2005; *Ellison et al*., 2006] attributed to a more sustained LIS meltwater drainage [*Keigwin et al*., 2005].

[5] High-frequency climate variability has also been investigated using modelling approaches. As a consequence of a freshwater induced pulse such as during the 8.2 ka cooling event, *Renssen et al*. [2002] detected a weakening of the thermohaline circulation and an increase of freshwater input due to extended sea-ice coverage and therefore a lowered density of surface waters.

[6] An increasing number of studies points to several cooling events during the Holocene [*Bond et al*., 1997, 2001; *Bianchi and McCave*, 1999; *Chapman and Shackleton*, 2000; *McDermott et al*., 1999; *Schulz and Paul*, 2002; *Wanner et al*., 2011] that are not clearly reflected in Greenland ice core records. Although millennial-scale cyclicity possibly caused by solar output was proposed [e.g., *Bond et al*., 2001], no consistent evidence for significant Holocene climate cyclicity has been found so far in the northern North Atlantic [e.g., *Schulz et al*., 2004; *Wanner et al*., 2011].

[7] The purpose of this study is to reconstruct the Holocene variability of Atlantic-derived heat transfer to the Arctic Ocean, by expanding the records from recently published work on the climate and paleoceanographic development during the past two millennia in the eastern FS [*Spielhagen et al*., 2011; *Werner et al*., 2011] to the past ~8.8 ka. Several studies have revealed that the multiyear warming events of AW in the FS and Arctic in the last decades went along with significant increases of AW advection by volume to the Arctic [*Dickson et al*., 2000; *Karcher et al*., 2003; *Schauer et al*., 2004]. We hypothesize that this modern analog can be transferred to conditions in the last 9000 years which overall had quite similar interglacial conditions. Furthermore, we will compare Early and Mid- with Late (pre-industrial) Holocene variability of oceanic heat flux to the Arctic Ocean and the position of the sea-ice margin in the eastern FS. Compared to earlier studies [e.g., *Sarnthein et al*., 2003] we provide new insights to conditions of surface versus subsurface water masses by presenting stable isotope records of the planktic foraminifer species *Neogloboquadrina pachyderma* and *Turborotalita quinqueloba*. Together with benthic proxy data this allows us to reconstruct water mass properties covering the entire water column and assess potential links between surface and bottom waters.

2. Regional Hydrography

[8] Two major current systems characterize the hydrographical configuration in the FS (Figure 1): (1) The West Spitsbergen Current (WSC) and (2) the East Greenland Current (EGC). The WSC carries warm (summer temperatures 6 to 7°C) and saline (up to 35.2) AW derived from the North Atlantic Drift to the Arctic Ocean through eastern FS [*Schauer et al*., 2004]. The main heat transport occurs within the core of AW, which is confined to the upper part of the continental slope off Svalbard [*Saloranta and Haugan*, 2004]. Since the WSC is topographically guided along the Barents Sea and Spitsbergen continental slopes [*Gammelsrød and Rudels*, 1983], it also entrains polar water from the Barents Sea, which is anticyclonically transported to the south and west around southern Spitsbergen by the East Spitsbergen Current (ESC) [*Hopkins*, 1991]. North of ca 78°N, close to our study site (Figure 1), the WSC submerges below colder and low-saline water of Arctic origin and continues as a subsurface current into the Arctic Ocean [*Johannessen*, 1986]. The western FS is perennially covered by sea ice. The EGC transports cold and fresh polar waters ($T < 0°C$, $S < 34.4$) [*Schlichtholz and Houssais*, 1999; *Rabe et al*., 2009] and sea ice southward along the Greenland margin.

[9] Over the last ~150 years, the sea-ice extent in the FS has varied significantly [*Vinje*, 2001] (Figure 1). The sea-ice distribution in the FS is mainly controlled by the outflow of Arctic waters and the intensity of AW which today provides ice-free conditions during most of the year in the eastern part of the strait [*Vinje*, 2001] (Figure 1). Where the WSC and EGC pass each other in opposite directions, meso-scale eddies are generated which carry AW westward across the FS [*Johannessen*, 1987]. This part of the AW submerges in the central and western FS beneath the cold, ice-covered EGC waters and flows southward at intermediate depths as the Return Atlantic Current [e.g., *Gascard et al*., 1988] (Figure 1).

[10] In deeper layers, Arctic Intermediate Water [*Marnela et al*., 2008], Norwegian Sea Deep Water [*Schlichtholz and Houssais*, 1999] and Greenland Sea Deep Water [*Schauer*, 1989; *Hebbeln*, 1991] are transported to the Arctic Ocean.

3. Material and Methods

[11] The 977 cm long kastenlot core MSM5/5-712-2 was obtained from the western Svalbard continental margin (78°54.94'N, 6°46.04'E, 1490.5 m water depth; Figure 1) during cruise leg MSM5/5 with RV "Maria S. Merian" in summer 2007. The uppermost 212 cm discussed here consist of olive grayish fine-grained muds apparently representing continuous sedimentation. Age control is based on ten accelerator mass spectrometry (AMS) radiocarbon dates

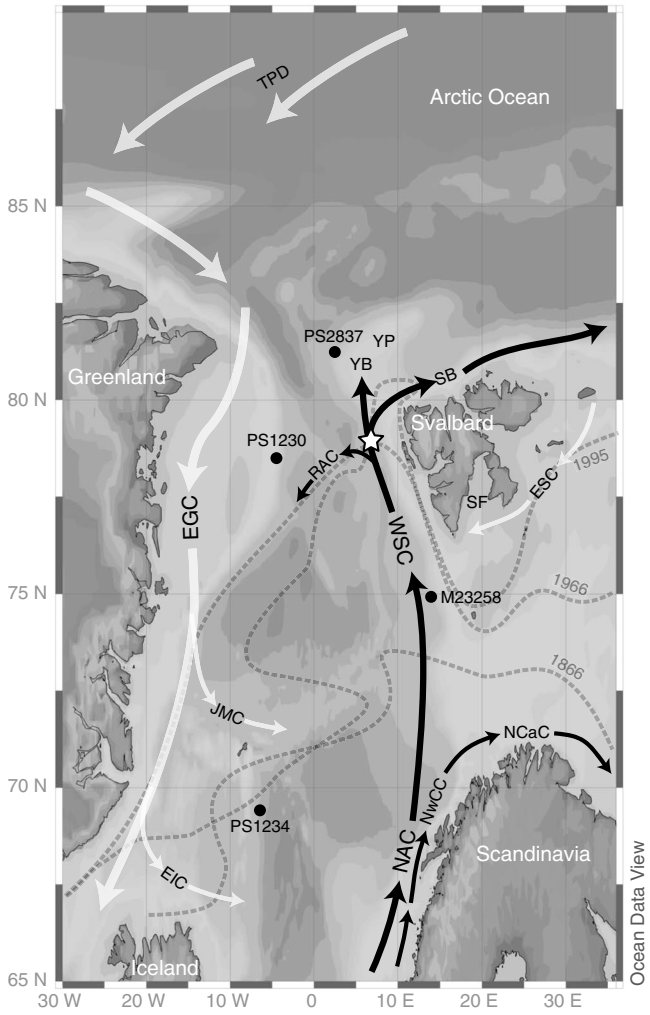

Figure 1. The Fram Strait and northern Nordic Seas with main surface/subsurface water currents. Black arrows indicate inflow of warm and saline Atlantic Water to the Arctic Ocean via eastern Fram Strait. White arrows mark cold and low-saline waters of Arctic origin. Core site MSM5/5-712-2 is marked by a white star. Indicated with black dots are core locations PS1230 and PS1234 [*Bauch et al*., 2001a], PS2837 [*Hass*, 2002], and M23258 [*Sarnthein et al*., 2003]. Also shown are selected extreme positions of the sea-ice margin (dashed lines with year specification) within the past 150 years after *Vinje* [2001]. EGC = East Greenland Current, EIC = East Iceland Current, ESC = East Spitsbergen Current, JMC = Jan Mayen Current, NAC = North Atlantic Current, NCaC = North Cape Current, NwCC = Norwegian Coastal Current, RAC = Return Atlantic Current, SB = Svalbard Branch, SF = Storfjorden, TPD = Transpolar Drift, WSC = West Spitsbergen Current, YB = Yermak Branch, YP = Yermak Plateau.

(for details see *Müller et al*. [2012]). All ages are given in 10^3 calender years (ka) before 1950 CE.

[12] The core was sampled every cm between 10.5 and 211.5 cm core depth. Samples used for analyses of coarse fraction content (weight-% >63μm), stable isotope measurements, and planktic foraminiferal assemblages were freeze-dried and wet-sieved in deionized water through a 63 μm-sized mesh to remove clay and silt material. Dry bulk density was determined from defined 10 cm^3 samples (10 ml syringes) at a 5 cm interval in the uppermost 50 cm and at 10 to 15 cm intervals in the remaining core section. Analyses of coarse fraction content and sortable silt mean grain size, as well as stable isotope measurements on the planktic foraminifer species *N. pachyderma* and the benthic foraminifer species *Cibicidoides wuellerstorfi* were conducted in 1 cm steps. Stable isotope measurements on the planktic foraminifer species *T. quinqueloba* were carried out every 5 cm and every 1 cm in selected intervals. Planktic foraminiferal assemblages in size fraction 100–250 μm were studied in 1 and 2 cm intervals.

[13] Stable oxygen and carbon isotope analyses were performed on ca 25 calcareous tests of *N. pachyderma* ($\delta^{18}O_{Np}$, $\delta^{13}C_{Np}$) and *T. quinqueloba* ($\delta^{18}O_{Tq}$, $\delta^{13}C_{Tq}$), and on ca 15 tests of *C. wuellerstorfi* ($\delta^{18}O_{Cw}$, $\delta^{13}C_{Cw}$). In order to prevent possible ecological biases of different morphotypes [*Healy-Williams*, 1992] only four-chambered ("square-shaped") specimens of *N. pachyderma* were used. The tests were crushed and mingled so that well-mixed aliquots could be used for the measurements. Stable isotope analysis was carried out using a Finnigan MAT 253 mass spectrometer system and a Kiel IV Carbonate Preparation Device at the GEOMAR Stable Isotope Lab. The carbonate was treated with orthophosphoric acid at 70°C. The analytical accuracy was <0.06‰ for $\delta^{18}O$ and <0.03‰ for $\delta^{13}C$. All measurements were calibrated to Pee Dee Belemnite using NBS 19. $\delta^{18}O$ data of *C. wuellerstorfi* were corrected for their vital effect by +0.64‰ [*Shackleton and Opdyke*, 1973; *Duplessy et al*., 2002]. Ice-volume corrected $\delta^{18}O_{(ivc)}$ data were calculated with an ice-volume component of 1.05‰ [*Duplessy et al*., 2002] and a sea level 120 m lower than today during the Last Glacial Maximum [*Fairbanks*, 1989].

[14] A representative split of at least 300 planktic foraminiferal tests was counted in size fraction 100–250 μm and identified to species level. Based on planktic foraminifer counts in size fraction 150–250 μm, subsurface temperatures (SST, July-September) at 50 m water depth were calculated using the SIMMAX modern analogue technique [*Pflaumann et al*., 1996, 2003]. To increase the precision of our SST estimates the core-top reference data set was restricted to the North Atlantic following the strategy of *Kucera et al*. [2005]. This method has successfully met the average modern water temperature at 50 m depth by a temperature reconstruction from planktic foraminifers in the sediment surface sample (6°C) [*Spielhagen et al*., 2011]. Planktic foraminifer fluxes were calculated based on dry bulk density values and linear sedimentation rates.

[15] To calculate variations in summer sea subsurface salinities (SSS) we followed the procedure by *Werner et al*. [2011]. A modern salinity/$\delta^{18}O$ correlation of the water column on the Western Svalbard margin (100–500 m water depth) was obtained by data from *Frank* [1996] and *Meredith et al*. [2001], retrieved from the Global Seawater Oxygen-18 Database [*Schmidt et al*., 1999; see also Figure 2 in *Werner et al*., 2011]. Salinity calculations were corrected by a shift of −0.2 ‰ in foraminiferal $\delta^{18}O$ to account for advection of tests from potentially warmer regions. This correction was used for salinity calculation only [for details, see *Werner et al*., 2011].

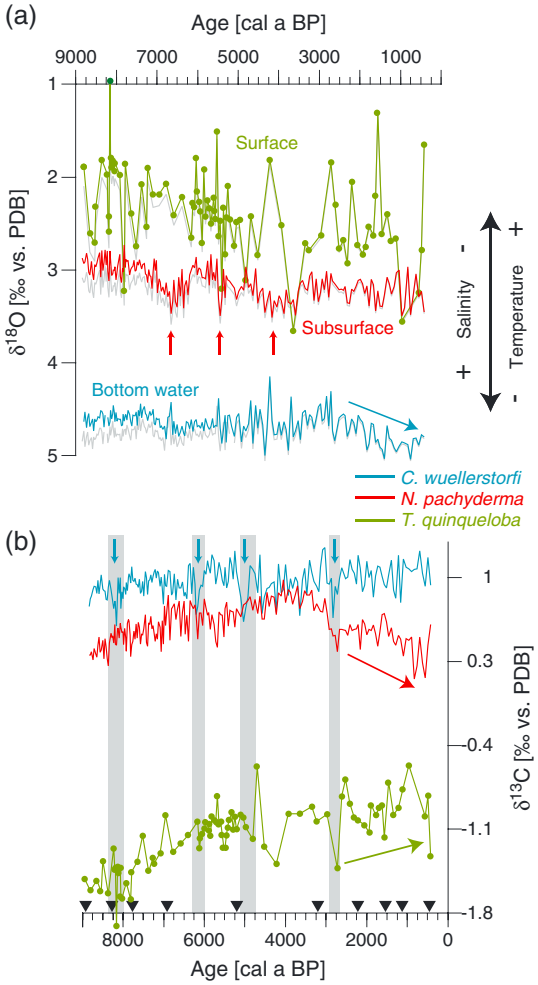

Figure 2. (a) Ice-volume corrected planktic and benthic $\delta^{18}O$ records from site MSM5/5-712-2. Uncorrected data is shown in gray color behind the records. $\delta^{18}O$ data of *C. wuellerstorfi* were corrected for their disequilibrium effect [−0.64; *Duplessy et al.*, 2002] (b) $\delta^{13}C$ records of planktic and benthic foraminifera. Arrows and shaded areas mark certain events and trends referred to in the text. Black triangles indicate AMS ^{14}C datings.

[16] Calculated SSS are based on both SST and measured planktic $\delta^{18}O$ values of *N. pachyderma*. We understand SST and SSS values as a translation of planktic foraminifer fauna and $\delta^{18}O_{Np}$ data and refrain from interpreting absolute values. Translated salinities display those of the ambient planktic foraminifer habitat but not of the actual sea surface. As the planktic foraminifer species *N. pachyderma* lives in subsurface waters [50–200 m; *Bauch et al.*, 1997], presented salinities rather reflect subsurface water conditions (this applies also to $\delta^{18}O_{Np}$). High amplitudes in salinity changes are thus interpreted in terms of water mass changes. Also, only salinity trends are interpreted since extrema could be caused by additional glacial melt water that would change any applied $\delta^{18}O$/salinity correlation.

[17] Aliquots of freeze-dried bulk sediment samples were used for the analysis of sortable silt mean grain size ($\overline{SS}$). To remove carbonate and organic matter, samples were treated with acetic acid and hydrogen peroxide, respectively. After adding sodium polyphosphate for better dispersion, the freeze-dried samples were put on a shaker for at least 24 h. Measurements were performed with a CILAS 1180L laser-diffraction particle analyser. The sortable silt size mean grain size 10–63 µm [*Robinson and McCave*, 1994] was calculated using the entire granulometric data sets based on vol.%.

4. Results

4.1. Planktic and Benthic Stable Isotopes

[18] Ice-volume corrected planktic and benthic $\delta^{18}O$ data show high fluctuations throughout the record (Figure 2a). Planktic $\delta^{18}O$ values of *N. pachyderma* vary between 2.7 and 3.5‰. Particularly, heavy $\delta^{18}O_{Np}$ values (~3.5‰) are noticed around 6.6, 5.4, and between 4.5 and 3.5 ka. $\delta^{18}O_{Tq}$ values highly fluctuate between 1.0 and 3.6‰ (Figure 2a). Highest variability in $\delta^{18}O_{Cw}$ data is seen between 5 and 4 ka ranging between 4.1 and 5.0‰. After 2.8 ka, heavier $\delta^{18}O_{Cw}$ values are noticed (Figures 2a and 3a).

[19] $\delta^{13}C$ values of *N. pachyderma* gradually increase until ~4 ka to maximum values of ~1.0‰ and decrease thereafter (Figure 2b). In contrast, $\delta^{13}C_{Tq}$ data reveal a trend to heavier values throughout the record, albeit with strong fluctuations between −1.9 and −0.6‰ (Figure 2b). Similarly, benthic $\delta^{13}C$ data (between 0.6 and 1.3‰) show a trend to

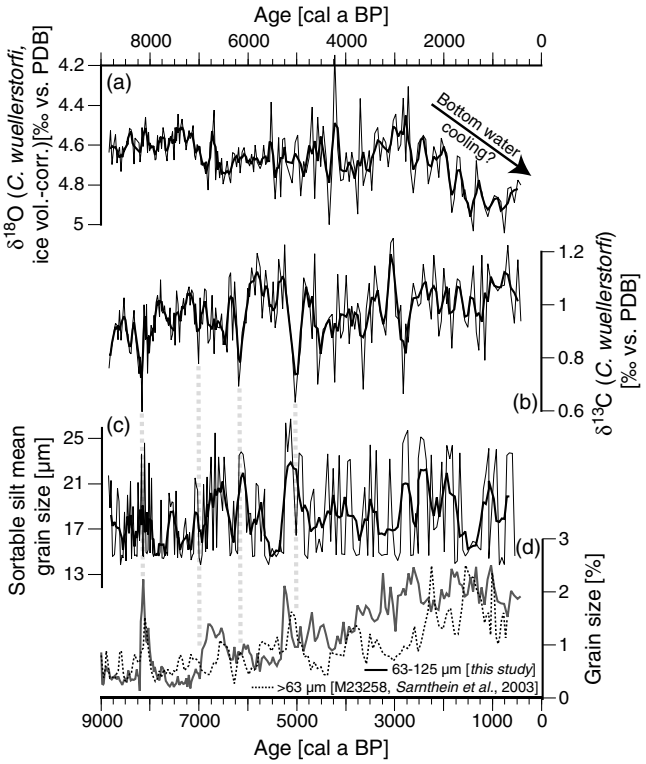

Figure 3. (a) Ice-volume corrected $\delta^{18}O$ record of *C. wuellerstorfi*. (b) $\delta^{13}C$ record of *C. wuellerstorfi*. (c) Sortable silt mean grain size. (d) Coarse-grain size records from presented site MSM5/5-712-2 and site M23258 [*Sarnthein et al.*, 2003]. Thick lines mark (a and b) three-point moving averages and (c) five-point moving averages. Gray dashed lines highlight coeval excursions of $\delta^{13}C_{Cw}$, sortable silt data, and grain size records.

heavier values during the entire studied period (Figures 2b and 3b). Short-term minima in all $\delta^{13}C$ data are noted at 8.2, 6.1, 5.0, and 2.9 ka (Figure 2b).

4.2. Planktic Foraminifer Assemblages and Fluxes

[20] In the notation, we follow *Darling et al*. [2006] who showed that sinistral and dextral coiling *N. pachyderma* are two different species. Accordingly, we use the suggested new terms *N. pachyderma* and *Neogloboquadrina incompta*, respectively. Records of *Globigerinita uvula* and *Globigerinita glutinata* are presented combined in one record as *Globigerinita* spp. (Figure 4c).

[21] *Turborotalita quinqueloba* dominates the planktic foraminiferal assemblages from ~9 to 5.2 ka, in particular before 8.2 ka (up to 75%; Figure 4b). Large proportions of *N. pachyderma*, commonly regarded as the only species reflecting polar surface water [*Bauch et al*., 2001a], are seen between 8.2 and 8.0 (up to 68%), between 7 and 5.9 ka (60 to 88%) with peaks at 6.9 and 6.1 ka, and after 5.2 ka (>90%; Figure 4b). A local maximum of *T. quinqueloba* up to 40% is observed at 6.5 ka. After 5.2 ka *T. quinqueloba* dropped to values mostly <20%. Slight increases of *T. quinqueloba* are noticed around 3 ka and at 1.9 ka (Figure 4b). Proportions of *Globigerinita* sp. were larger between 8 and 5 ka (up to 6%) and increased up to 17% within the past 3 ka (Figure 4c).

[22] Before 7.3 ka, planktic foraminifer fluxes had maximum values (up to 32,000 ind./cm^2*ka; Figure 4f). Between 5 and 3.5 ka fluxes were low but slightly increased again after 3.5 ka.

4.3. Sea Subsurface Temperatures and Salinities

[23] Calculated SST and SSS fluctuate strongly between 8.8 and 5.2 ka but reveal generally relatively warm and saline subsurface conditions (>5°C and >34.5psu; Figures 4d–4e). Until 7 ka, temperatures/salinities strongly vary. At 6.9 and 6.1 ka, SST and SSS were lowest (<2°C and <33) but increased thereafter (up to 5.6°C and >34.5). After 5.2 ka, SST drastically decreased (1.2°C) and remained low until ~3.5 ka. A gradual temperature increase is noticed at ~3 and 1.5 ka.

4.4. Sortable Silt Mean Grain Size

[24] The sortable silt mean grain size ($\overline{SS}$) varies between 14 and 27 μm in the studied core section (Figure 3c). $\overline{SS}$ data have been checked for IRD contamination following *Hass* [2002] and reveal an insignificant influence of ice-transported silt. However, since the core location is close to land, episodes of ice rafting during colder periods may have caused deposition of ice-rafted silt that was not accompanied by coarser material that is thus hard to detect. Higher amounts of coastal sea ice carrying finer materials from shallow areas might be responsible for altered IRD signals in short-term cold episodes. Various effects of different bottom currents and their entrained sediments complicate the interpretation of $\overline{SS}$ data. We therefore focus on the main trends shown in the five-point moving average (Figure 3c). Higher $\overline{SS}$ values are observed from 7 to 6 ka, around 5 ka, and from 3 to 1.8 ka. We note that opposite trends of $\delta^{13}C_{Cw}$ and $\overline{SS}$ values occur in particular during the late Early and Mid-Holocene intervals (Figures 3b–3c).

5. Discussion

5.1. Climate Conditions During Late Early to Mid-Holocene (8.9 to 5.2 ka)

[25] Large proportions of the planktic foraminifer species *T. quinqueloba* and reconstructed similar-to-present SST (up to 6°C) and SSS (>35.1) characterize the late Early and Mid-Holocene intervals (8.9-5.2 ka) at site MSM5/5-712-2 (Figures 4b, 4d–4e). *Turborotalita quinqueloba* is the second most abundant planktic foraminifer species in eastern FS sediments and is abundant in AW masses nearby the marginal ice zone [*Carstens et al*., 1997; *Volkmann*, 2000]. According to the modern analog of coeval changes in AW advection and temperatures [*Dickson et al*., 2000; *Karcher et al*., 2003; *Schauer et al*., 2004], large proportions of *T. quinqueloba* can be attributed to intense and warm AW advection to the eastern FS. We thus interpret the *T. quinqueloba* relative abundance record in terms of AW temperatures and inflow strength of this water mass. Increased heat flux to the Arctic Ocean during the Early Holocene has been related to the insolation maximum in the northern hemisphere [e.g., *Koç et al*., 1993; *Bauch et al*., 2001a; *Hald et al*., 2007; *Risebrobakken et al*., 2010]. The insolation maximum in the northern hemisphere concurred with warmest Holocene atmospheric temperatures, as documented in Greenland ice cores [*Stuiver et al*., 1995; *Rasmussen et al*., 2006; *Vinther et al*., 2006] (Figure 4a) and terrestrial proxy records [e.g., *Svendsen and Mangerud*, 1997; *Seppä and Birks*, 2001; *Humlum et al*., 2005]. We therefore conclude on generally warm Early Holocene conditions from our *T. quinqueloba* abundance record.

[26] Parallel to the decrease in insolation (Figure 4a), we find a gradual cooling trend indicated by slightly decreasing *T. quinqueloba* proportions after 8 ka (Figure 4b). *Carstens et al*. [1997] showed that highest particle fluxes are related to maximum bioproductivity at the sea-ice margin in the FS. Accordingly, we link high planktic foraminifer fluxes ~8 ka (Figure 4f) either to ice-free conditions or the sea-ice margin seasonally fluctuating over the study site. Lower reconstructed SST and heavier $\delta^{18}O_{Np}$ after 7 ka are likely related to cooler temperatures in subsurface water masses (Figures 4e and 4h).

[27] Our results corroborate earlier evidence for strong AW advection to the Svalbard area during the Early Holocene. From planktic foraminiferal investigations on core M23258 (75°N, south of Svalbard), *Sarnthein et al*. [2003] concluded on relatively warm conditions lasting until ~7 ka, similar to our record (Figure 4b). This is also consistent with Holocene foraminiferal studies in the Barents Sea [*Duplessy et al*., 2001; *Risebrobakken et al*., 2010], around Svalbard [*Rasmussen et al*., 2007, 2012; *Ślubowska-Woldengen et al*., 2008], and in the Nordic Seas [*Bauch et al*., 2001a], which indicate Mid-Holocene thermal maximum conditions until ~7 ka and a pervasive surface cooling thereafter. *Risebrobakken et al*. [2011] disentagled the influences of oceanic heat advection and insolation for the Early Holocene warming in the Nordic Seas. They found that oceanic heat advection peaked around 10 ka while maximum warming of the surface mixed layer occurred from 9 to 6 ka. Our results are not contradictory but reveal more details of the decreasing trend in AW temperatures (and probably strength). In particular, we note the rapid temperature decrease by 3.5°C between 7.2 and 7.0 ka (Figure 4e), at

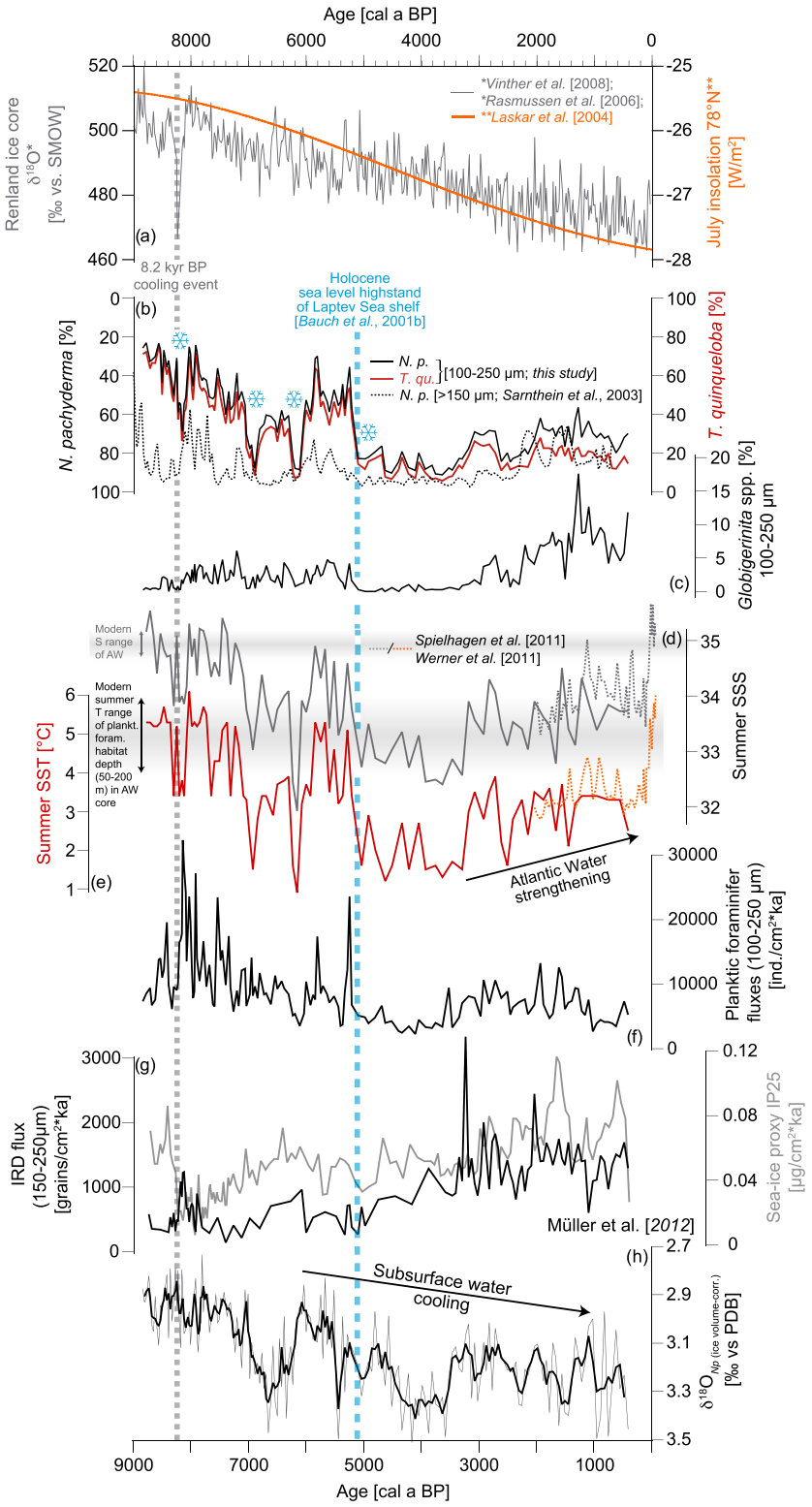

Figure 4. (a) Greenland ice core data and solar irradiance. (b) Percentages of planktic foraminifer species *N. pachyderma* (100–250 µm, black solid line) and *T. quinqueloba* (dark red line). Short-lived coolings indicated by sudden temperature drops are marked with ice crystals. Also shown is the record of *N. pachyderma* from the Western Barents Sea [*Sarnthein et al.*, 2003] in size fraction >150 µm (black stippled line). (c) Combined record of *G. uvula* and *G. glutinata* as *Globigerinita* spp. (100–250 µm). (d–e) Calculated summer sea subsurface salinities and temperatures (at 50 m water depth) (f) Planktic foraminifer fluxes in size fraction 100–250 µm. (g) Ice-rafted debris and sea-ice indicative biomarker data from Müller et al. [2012] (h) Ice-volume corrected $\delta^{18}O$ record of *N. pachyderma*.

the very end of the Early Holocene. This reduction is hardly compatible with a gradually decreasing strength of AW advection and may be related to other environmental changes in the Arctic, discussed further below.

[28] Our planktic foraminiferal and SST data reveal a Mid-Holocene warm interval between 6.1 and 5.2 ka in the eastern FS (Figures 4b and 4e), similar to records from the Western Barents Sea and the Lofoten Basin [*Bauch and Weinelt*, 1997; *Sarnthein et al*.; 2003] (Figure 4b). However, our data indicate this interval did not reach the high temperatures of the late Early Holocene. In accordance with *Hald et al*. [2007], we relate this strong warming signal in our record to the amplification of warm conditions in FS caused by an insulating meltwater coverage and limited heat loss to the atmosphere [*Haugan*, 1999].

[29] Benthic $\delta^{18}O$ values of *C. wuellerstorfi* (Figure 2a) are relatively constant from 9 to 5 ka, probably indicating stable deepwater conditions. Concurrent to increasing total organic carbon contents at site MSM5/5-712-2 [*Müller et al*., 2012], $\delta^{13}C$ values of all three investigated foraminifer species reveal increasing trends (Figure 2b). This indicates a general increase of surface productivity during this part of the Holocene. In the Arctic realm, heavy planktic $\delta^{13}C$ values have also been attributed to well-ventilated water masses [e.g., *Spielhagen and Erlenkeuser*, 1994]. Gradually, better ventilation of the entire water column might thus serve as another reason for increasing $\delta^{13}C$ data during the late Early and Mid-Holocene.

[30] In addition, we present an alternative explanation for the trend to heavier planktic $\delta^{13}C$ values. It has been shown that depth preferences of the foraminifer species *N. pachyderma* and *T. quinqueloba* in the FS depend on surface water conditions [*Carstens et al*., 1997; *Kozdon et al*., 2009]. *Carstens et al*. [1997] found a gradual deepening of the main habitat of planktic foraminifers from eastern (50–150 m) to western (below 150 m) FS, related to a preference of the planktic foraminifers for the warm AW that submerges in western FS below low-saline and cold Arctic water masses and is found in greater depths in the western FS within the Return Atlantic Current. Accordingly, *Kozdon et al*. [2009] suggested that the average depth of *N. pachyderma* is controlled by water density. Either dependent on the depth of AW or on the density distribution of the water column, planktic foraminifers calcify in greater water depths under sea-ice coverage (150–200 m) whereas under ice-free conditions and warmer sea surface temperatures their habitat depth is shallower [*Carstens et al*., 1997]. We therefore consider it possible that heavier planktic $\delta^{13}C$ values reflect conditions at shallower habitat depth due to the migration activity of planktic foraminifers. Reasons for a potential depth change during the late Early to Mid-Holocene may be related to surface water warming and changes in the distribution of surface water masses.

[31] While we prefer the explanation provided above, stepwise increasing planktic $\delta^{13}C$ values during the Early and Mid-Holocene in the Barents and Kara Seas have been explained by the deglacial/Holocene sea-level rise and a progressive increase in shelf area [*Lubinski et al*., 2001]. Continuous flooding of the exposed shelf areas in the Kara and Laptev Seas may have resulted in an increasing transport of well-ventilated shelf waters to the Arctic Ocean until sea level stabilized at ~6 C^{14}ka [*Lubinski et al*., 2001].

5.2. Repeated 8.2 ka-Like Coldwater Events During Late Early to Mid-Holocene (8.9 to 5.2 ka)

[32] Increases of *N. pachyderma* abundances at 8.2, 6.9, and 6.1 indicate short-lived coolings that repeatedly interrupted the relatively warm/saline conditions and strong AW advection to site MSM5/5-712-2 during the late Early and Mid-Holocene.

[33] The peak of *N. pachyderma* percentage at 8.2 ka is most likely related to the "8.2 ka event" [e.g., *Stuiver et al*., 1995; *Barber et al*., 1999; *Rohling and Pälike*, 2005]. In our record, this event is well pronounced and spans a 400-year interval, with most distinctive conditions at ~8.2 ka (Figure 4). From ~8.4 to 8.2 ka relative abundances of *T. quinqueloba* strongly decreased from >60 to 26% and the polar planktic species *N. pachyderma* became dominant (>68%; Figure 4b). Low SST and SSS, high planktic foraminifer fluxes and a strong increase in *N. pachyderma* proportions, as well as a short-lived doubling of IRD contents and sea-ice indicating biomarker data [*Müller et al*., 2012] (Figure 4g) point to increased sea-ice/iceberg rafting and an advance of the sea-ice margin over the study site. $\delta^{18}O$ data of *T. quinqueloba* exhibit depleted values (ca 1.0‰) around 8.2 ka (Figure 2a), potentially linked to an increased freshwater influence in the surface layer. After 8.1 ka, *T. quinqueloba* proportions rise again to values of >60% (Figure 4b).

[34] A short strong decrease in benthic $\delta^{13}C_{Cw}$ suggests that the deepwater was also affected during the 8.2 ka event (Figure 3b). Short-lived decreases in benthic $\delta^{13}C$ in the Nordic Seas around 8 ka have been assigned to decreased bottom water ventilation possibly due to an entrainment of relatively fresh water into the thermohaline system [*Bauch et al*., 2001a]. Based on sedimentological data from the western Yermak Plateau slope (core PS2837, 1042 m water depth; Figure 1), *Hass* [2002] proposed more sluggish bottom water circulation along the western Svalbard-Yermak Plateau slope, linked to a slow-down of the MOC during the 8.2 ka event (Figure 5).

[35] We would expect a correlation between light $\delta^{13}C_{Cw}$ values and decreased sortable silt values for the 8.2 ka event. However, the outstanding minimum in the $\delta^{13}C_{Cw}$ record relates to peak $\overline{SS}$ values (Figures 3b–3c). The reason for this anticorrelation may be related to the geographic setting of our investigated site. Core MSM5/5-712-2 was obtained downslope of Kongsfjorden and Kongsfjordrenna, one of the major outlet systems of western Svalbard. Enhanced sea-ice formation during the cold 8.2 ka event may have led to strong formation of dense brine waters ("winter water") in the fjord/trough system which could carry somewhat coarser sediment material downslope. To explain the origin of coarser-grained layers [>63 μm] in core M23258 from the western Barents Sea margin (75°N; Figures 1 and 3d), *Sarnthein et al*. [2003] proposed a similar process. They concluded that heavy sea-ice conditions and cascades of sediment-bearing dense brine waters resulted in a series of increased lateral sediment injections to their site episodically in the last 8.8 ka. In our core, we find largely coeval grain size excursions [63–125 μm] for the 9–5 ka interval (Figure 3d). These findings point to a similar process of formation and a link between climate deteriorations and sediment events on the Barents shelf and on the western Svalbard margin

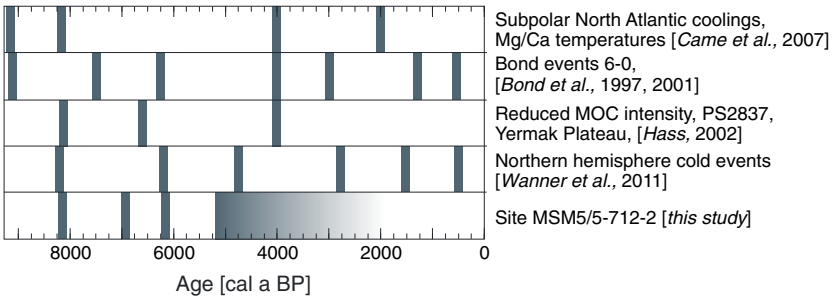

Figure 5. Coolings reconstructed from site MSM5/5-712-2 in comparison to those compiled from the literature.

(Figure 3d). In our record benthic $\delta^{18}O$ values show no response to the $\overline{SS}$ record. If the $\overline{SS}$ record reflects sediment transport related to brine formation, benthic $\delta^{18}O$ values may only respond if surface waters were depleted in $\delta^{18}O$ (Bauch and Bauch, 2001).

[36] Other short-lived coolings occurred at 6.9 and 6.1 ka and are most prominently seen in significant increases in *N. pachyderma* percentages of up to >88% (Figure 4b). Similar to the 8.2 ka event, the cooling in surface water masses at 6.1 ka was accompanied by increased $\overline{SS}$ values and minimum $\delta^{13}C_{Cw}$ values (Figures 3b and 3c).

[37] Short-term cooling events in the North Atlantic region have been reconstructed from various Holocene records (Figure 5). From repeated ice-rafting events south of Iceland, *Bond et al.* [1997, 2001] concluded on a near-1500-year Holocene cyclicity in the North Atlantic influenced by solar-induced atmospheric variations. Bond events 5 and 4 [*Bond et al.*, 1997] may correspond to the cooling events detected at site MSM5/5-712-2 in the eastern FS at 8.2 and 6.1 ka (Figure 5), but correlatives to other IRD events are not found. *Came et al.* [2007] noticed abrupt events in the subpolar North Atlantic but except for the 8.2 ka event, the timing of events recorded by these authors differs significantly from those at site MSM5/5-712-2 (Figure 5). Distinct similarities exist between our coolings and the cold relapses at 8.2 ka and between 6.5 and 5.9 ka detected by means of statistical analysis of proxy time series by *Wanner et al.* [2011] (Figure 5). The authors showed that several cold events, which interrupted periods of relatively stable and warmer climate during the Holocene, did not follow a strictly regular or cyclic appearance but suggested that the complex pattern of these short-term coolings was caused by a combination of decreasing solar insolation, possibly a slow-down of the MOC, regional effects, and feedbacks. For the eastern FS, we consider repeated advances and retreats of the sea-ice margin to be most important for the strong changes in surface and subsurface water conditions during the late Early and Mid-Holocene. Advances of the Arctic Front, i.e., the boundary between Atlantic and Arctic water masses [*Johannessen et al.*, 1994], serve as the best explanation for the strong shifts in surface ocean conditions. Correlating our surface water coolings to glacier advances on Svalbard is difficult due to the lack of sufficient high-resolution records from Svalbard. However, evidence for possible glacier growth starting ~7 ka and a general increase in glacier-related iceberg rafting between 9 and 4 ka has been found in Isfjorden, West Svalbard [*Forwick and Vorren*, 2007, 2009].

5.3. Cold Conditions After ~5.2 ka

[38] The climate shift at 5.2 ka is characterized by a pattern similar to the short-lived cold events between 9 and 6 ka, with pronounced increases in *N. pachyderma*, low SST and SSS, high planktic foraminifer fluxes, and high IRD contents (Figure 4). However, this transition represents a cooling which differs from the otherwise observed 8.2 ka-like cooling events as it marks the onset to permanent Neoglacial conditions lasting throughout the remainder of the studied core section.

[39] Our findings are in agreement with colder conditions in the second half of the Holocene documented in various proxy reconstructions in the Nordic Seas [e.g., *Jennings et al.*, 2002; *Moros et al.*, 2004; *Seidenkrantz et al.*, 2008; *Andrews et al.*, 2009, 2010] but also found in a global context [*Wanner et al.*, 2008 and references therein]. *Svendsen and Mangerud* [1997] dated the first well-pronounced Neoglacial glacier formation in West Spitsbergen between 5 and 4 ka. Accordingly, glacier re-advances in western Norway [Nesje and Kvamme, 1991] and North America [*Denton and Karlén*, 1973] were determined to about 5.3 ka.

[40] *Wanner et al.* [2008] attributed the Neoglacial cooling in the northern hemisphere to the decreasing solar radiation, the southward shift of the Intertropical Convergence Zone, and hence, a summer cooling trend over the northern continental landmasses and the North Atlantic Ocean. Consistently, we conclude on a summer cooling trend for the Neoglacial period, which started rather abruptly in the eastern FS and was most probably related to an advance of the sea-ice margin over the study site at ~5.2 ka. The decrease of *T. quinqueloba* percentages from >50% to <15% within ~150 years indicates a strongly weakened AW inflow or a sudden drop of AW temperatures as inferred by foraminifera temperature estimates (Figure 4e). Decreases in *T. quinqueloba* percentages were also detected between 6 and 5 ka in the Storfjorden Fan [*Rasmussen et al.*, 2007] and in the Lofoten and western Norwegian Basins [*Bauch and Weinelt*, 1997]. We consider the combination of the advance of the sea-ice margin and low insolation as the most likely reason for the transition to prolonged cold conditions since 5.2 ka. Our results from the western Svalbard margin, close to the northernmost, partly glaciated land area bordering the eastern North Atlantic, indicate that the onset of Neoglacial cooling occurred rather rapidly in the far north.

[41] Minimum proportions of *T. quinqueloba*, low planktic foraminifer fluxes (Figures 4b and 4f), together with low biomarker accumulation rates [*Müller et al.*, 2012] point to restricted bioproductivity and intense sea-ice coverage between ~5 and 3 ka. Accordingly, heavier $\delta^{18}O_{Np}$ values since 5.2 ka

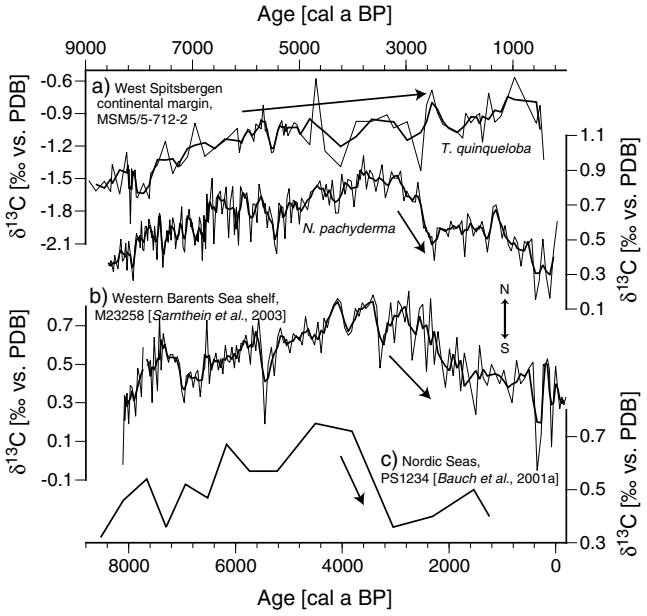

Figure 6. $\delta^{13}C$ records of *N. pachyderma* and *T. quinqueloba* from the subpolar North Atlantic and the Fram Strait.

likely reflect colder subsurface conditions (Figure 4h). The fact that fluctuations in $\delta^{18}O_{Tq}$ (Figure 2a) are much stronger than those in $\delta^{18}O_{Np}$ is probably related to rapid shifts in the habitat depths of *T. quinqueloba*, potentially caused by a variable thickness of the surface water layer. Evidence for the formation of a permanent ice cover and reduced iceberg and sea-ice drift after 4 ka in Isfjorden, West Svalbard [*Forwick and Vorren*, 2009] corroborates our conclusion on colder surface conditions since 5.2 ka.

[42] An increase of *Globigerinita* spp. (and of *G. uvula*, data not shown) after 3.2 ka in our record (Figure 4c) is consistent with findings of higher numbers of *G. uvula* in coeval layers of two cores from the SW Svalbard margin [*Rasmussen et al*., 2007]. High abundance of *G. uvula* in core MSM5/5-712-2 points to increased contribution of cool productive coastal surface waters [*Husum and Hald*, 2012] during the Late Holocene. At the same time, rising planktic foraminifer abundances, suggesting higher productivity, as well as significantly increasing IRD contents and sea-ice indicative biomarker data (Figures 4f–4g) implies that site MSM5/5-712-2 was probably located in the area of the seasonally fluctuating ice margin during the Late Holocene. Increased IRD contents in Late Holocene sediments found at many sites in the Nordic Seas [e.g., *Jennings et al*., 2002; *Sarnthein et al*., 2003; *Moros et al*., 2006; *Rasmussen et al*., 2007; *Ślubowska-Woldengen et al*., 2008] and off southeast Greenland [*Williams*, 1993; *Andrews et al*., 1997; *Jennings et al*., 2002, 2011] are generally interpreted as evidence of regrowing ice sheets.

[43] $\delta^{13}C$ records from three different foraminifer species hold interesting information about changes in the water mass structure on the western Svalbard margin in the Late Holocene Neoglacial phase. Values of $\delta^{13}C_{Np}$ are gradually decreasing after ~3.5 ka while $\delta^{13}C_{Tq}$ and $\delta^{13}C_{Cw}$ data do not follow this trend (Figure 2c). The latter steadily increase until ~0.4 ka, suggesting either higher bioproductivity or better ventilation in surface and bottom water masses. Reasons for the decreasing trend of $\delta^{13}C_{Np}$ data during the past ~3 ka may be found in a density-driven downward migration of *N. pachyderma* [*Kozdon et al*., 2009] to less-ventilated subsurface waters due to a gradual thickening of the sea-ice derived surface layer and increased freshwater availability. This is in contrast to *T. quinqueloba*, which as a symbiont-bearing near-surface dweller is bound to seasonally open conditions [*Simstich et al*., 2003; *Kucera et al*., 2005] and may have stayed in the uppermost surface water masses. Decreases in $\delta^{13}C_{Np}$ since 4 to 3 ka have also been noted in records from the northern North Atlantic [e.g., *Bauch and Weinelt*, 1997; *Bauch et al*., 2001a; *Sarnthein et al*., 2003; *Jessen et al*., 2010; *Risebrobakken et al*., 2011] (Figure 6). We therefore speculate that the drop in $\delta^{13}C_{Np}$ indicates a wider distribution of a thickening sea-ice derived freshwater layer in the Nordic Seas and the FS during the Late Holocene Neoglacial phase.

[44] The trend towards lighter $\delta^{13}C_{Np}$ values after 3.5 ka runs parallel to a trend to heavier benthic $\delta^{18}O$ (about 0.4‰; Figure 2) that may either be related to a cooling of ~1.4°C or a ~0.8 salinity increase in bottom waters. Evidence for cooler and fresher bottom waters during the Late Holocene was concluded from benthic foraminiferal data on the western and northern Svalbard shelves [*Ślubowska-Woldengen et al*., 2007, 2008]. Heavier $\delta^{18}O_{Cw}$ could also indicate higher salinity of bottom waters that may be generated by dense water formation during winter sea-ice formation in southern and western Svalbard fjords [*Quadfasel et al*., 1988; *Schauer*, 1995; *Rudels et al*., 2005; *Rasmussen and Thomsen*, 2009]. However, more information is needed to further investigate the feature of heavier $\delta^{18}O_{Cw}$.

5.4. Underlying Causes for Stepwise Transition Between Holocene Thermal Maximum and Neoglacial Conditions

[45] For the abrupt onset of cool conditions in eastern FS at 5.2 ka, we propose an Arctic Ocean-related increased export of sea ice and freshwater from the north to be responsible for the Neoglacial cooling in eastern FS (section 5.4.1.). At the same time, increased proportions of *T. quinqueloba* (24-28%), and higher SST and SSS from 3.1 to 2.8 and at ~1.9 ka (Figures 4b, 4d–4e) indicate a slight strengthening of subsurface AW inflow and/or AW temperature increase. However, except for the last ~150 years [*Spielhagen et al*., 2011] *T. quinqueloba* never achieves the large proportions of the Early and Mid-Holocene during the Late Holocene. In support of our conclusions, Mg/Ca- based SST estimates in *N. pachyderma* from the same site in eastern FS show increasing SST since 3.2 ka with a maximum of 5°C at ~1.1 ka [*Aagaard-Sørensen*, 2011]. Evidence for increased AW inflow after 3 ka has also been found in the Franz Victoria Trough [*Lubinski et al*., 2001], in the Nordic Seas [*Hald and Aspeli*, 1997; *Risebrobakken et al*., 2003] and on the western Barents Sea shelf [*Sarnthein et al*., 2003]. Also, in agreement with increased AW inflow, a slight strengthening of the MOC after 3 ka was inferred based on an increase of *T. quinqueloba* percentages [*Sarnthein et al*., 2003].

5.4.1. Increased Export of Arctic Sea Ice

[46] Postglacial flooding of the Laptev Sea shelves was finalized ~5 ka when the modern sea level was reached [*Bauch et al*., 2001b]. By means of ostracod assemblages, *Cronin et al*. [2010] determined the onset of modern-like

conditions with perennial sea ice in the Arctic Ocean to ~6 to 5 ka consistent with high-latitude Neoglacial cooling and glacier advances. Thus, at ~5 ka, Arctic sea-ice production, which predominantly takes place on the shallow Arctic shelf areas, reached its modern dimension. Apparently, the dramatic shift in our planktic foraminiferal data at ~5.2 ka and the associated sea-ice advance over the study site coincide with the timing of the establishment of the modern sea level and Arctic sea-ice production. From driftwood analyses and modelling experiments, it was suggested that during the Mid-Holocene, enhanced riverine discharge of freshwater caused an eastward shift of the Transpolar Drift and strengthened sea-ice export through FS [*Dyke et al*., 1997; *Prange and Lohmann*, 2003]. *Funder et al*. [2011] used the presence of driftwood as a proxy for multiyear sea-ice on the East Greenland coast. After 6 ka, the authors found increased export of multiyear sea ice through FS arriving from North America. This increasing sea-ice export indicates more frequent occurrences of the negative Arctic Oscillation (AO) mode with a stronger Beaufort Gyre and weaker TPD.

[47] In the FS, which acts as a bottleneck for sea-ice export, the ice cover is bounded to the west by Greenland and can thus react to stronger ice production only by faster ice flow or by an expansion in (south-)easterly direction or both. While past ice-drift speeds or modes of AO are difficult to determine, our data point to a significant and persistent (south-)eastward movement of the sea-ice margin since the Mid-Holocene, eventually reaching the Svalbard continental margin at 79°N. The expansion of the ice cover in the FS resulted in a strong shift to cooler conditions at our study site after 5.2 ka, a time when low insolation and atmospheric temperatures amplified both Arctic sea-ice production and higher albedo effects. Prior to this Mid-Holocene shift, Arctic sea-ice production may have been somewhat limited by higher atmospheric temperatures caused by (1) high insolation (possibly amplified in the Arctic basin due to lowered albedo), (2) the reduced area for sea-ice production on the shallow Arctic shelves because of the lower sea level, and (3) a stronger influx of warmer AW masses.

[48] In a low-resolution record from site PS1230 in the western FS (Figure 1), relative abundances of *T. quinqueloba* in the 63–125 μm size fraction dropped from 9% to <1% at ~8 ka, followed by a strong dominance of *N. pachyderma* indicating cool conditions [*Bauch et al*., 2001a]. Higher-resolution records are still lacking for this area, but a repeated advance of EGC-derived sea ice and a cold-water front from the northwest towards the southeast may explain our findings of centennial-scale cold events in the eastern FS between 9 and 5 ka. While the western FS was already perennially sea-ice covered after 8 ka, the cold-water front eventually arrived in the eastern FS ~5.2 ka. Owing to the melting induced by AW inflow, seasonally ice-free conditions likely prevailed during the latter half of the Holocene with some restrictions, e.g., during the colder phase between ~5 and 3 ka and the Little Ice Age [*Werner et al*., 2011].

[49] Decreasing $\delta^{13}C_{Np}$ values found in subsurface waters the Nordic Seas and FS after 3 ka (Figure 6) might be related to increased Arctic sea-ice and fresh water export and associated density-driven downward movement of *N. pachyderma* and uptake of lower $^{13}C/^{12}C$ ratios in subsurface water masses. *Bauch et al*. [2001a] point out the link between decreasing $\delta^{13}C_{Np}$ and the development of the modern steep east-to-west temperature gradient, which results from the establishment of the "modern-type-circulation" in the Nordic Seas. Accordingly, we hypothesize that the modern east-west temperature gradient in the Nordic Seas and FS evolved only after the modern "Arctic sea-ice factory" was established and a strong export of Arctic sea ice and cold-water masses to the Nordic Seas could be initiated. Modern-type surface water stratification in the eastern FS, characterized by a relatively thick upper mixed layer could thus probably only have been developed in the course of the widespread Late Holocene freshening in the northern North Atlantic [*Bauch and Weinelt*, 1997].

6. Conclusions

[50] Multiproxy data from the West Spitsbergen continental margin covering the past ~9 ka suggest that the transition from late Early Holocene thermal maximum conditions to the pre-industrial situation occurred stepwise, most likely in response to the postglacial flooding of the shallow Siberian shelves and the onset of modern sea-ice production. Planktic foraminifer assemblages, SST, and SSS data infer generally strong AW inflow and/or increased surface water temperatures concurrent to high insolation between 9 and 5 ka. A slight weakening of AW inflow is noted after 8 ka, but continuously high percentages of subpolar planktic foraminifer species indicate generally strong AW advection lasting until ~5 ka. Repeated short-lived events characterized by cold surface water interrupted the warm AW inflow in the eastern FS at 8.2, 6.9, and 6.1 ka.

[51] Neoglacial conditions were more stable but significantly cooler than during the Early and Mid-Holocene and established only after an abrupt transition to permanently cold conditions at 5.2 ka. Strong discharge of Arctic sea ice and polar waters transported southeastward by the ice-covered EGC caused heavy winter sea-ice conditions and relatively short ice-free summer seasons in the eastern FS, most likely in combination with a cooler and weaker subsurface AW inflow during the Late Holocene. A slight re-strengthening of AW inflow after 3 ka is seen from planktic foraminifer assemblages and calculated SST/SSS. During the past ~3 ka, increasing abundance of sea-ice transported material and decreasing planktic $\delta^{13}C$ values, also known from other records in the northern North Atlantic, indicate a freshening of the uppermost surface water layer. We hypothesize that the modern steep east-west temperature gradient in the FS and possibly the Nordic Seas only evolved after the modern "Arctic sea-ice factory" was established and a strong export of Arctic sea ice and cold and fresh surface water masses through FS could be initiated.

[52] **Acknowledgments.** We thank the science party and crew onboard RV "Maria S. Merian" during the expedition MSM5/5 for retrieving the sediment core. Furthermore, we are grateful to Jacques Giraudeau (University Bordeaux, EPOC) for providing three AMS datings. For laboratory assistance, we thank Torben Struve, Jan Oesterwalbesloh, and Marieke Göser. We kindly acknowledge Lulzim Haxhiaj for technical assistance on stable isotope measurements and Ethan Jewett for checking the language. This article greatly benefited from the constructive reviews by Heinz Wanner and three anonymous reviewers. The German Research Foundation (DFG) provided financial support of K. Werner and R.F. Spielhagen within the Priority Programme 1266 (INTERDYNAMIC, Project HOVAG). Supplementary data are available at http://dx.doi.org/10.1594/PANGAEA.810415.

References

Aagaard-Sørensen, S. (2011), Late Glacial - Holocene climatic variability and sedimentary environments on northern continental shelves, PhD thesis, Univ. of Tromsø, Tromsø, Norway.

Alley, R. B., P. A. Mayewski, T. Sowers, M. Stuiver, K. C. Taylor, and P. U. Clark (1997), Holocene climatic instability: A prominent, widespread event 8200 yr ago, *Geology*, *25*(6), 483–486.

Andrews, J. T., L. M. Smith, R. Preston, T. Cooper, and A. E. Jennings (1997), Spatial and temporal patterns of iceberg rafting (IRD) along the East Greenland margin, ca. 68°N, over the last 14 cal. ka, *J. Quat. Sci.*, *12*, 1–13.

Andrews, J. T., S. T. Belt, S. Olafsdottir, G. Massé, and L. L. Vare (2009), Sea ice and marine climate variability for NW Iceland/Denmark Strait over the last 2000 cal. yr BP, *Holocene*, *19*(5), 775–784.

Andrews, J. T., A. E. Jennings, G. C. Coleman, and D. D. Eberl (2010), Holocene variations in mineral and grain-size compositioin along the East Greenland glaciated margin (ca 67°-70°N): Local versus long distance sediment transport, *Quat. Sci. Rev.*, *29*, 2619–2632.

Barber, D. C., et al. (1999), Forcing of the cold event of 8,200 years ago by catastrophic drainage of Laurentide lakes, *Nature*, *400*, 344–348.

Bauch, D., J. Carstens, and G. Wefer (1997), Oxygen isotope composition of living *Neogloboquadrina pachyderma* (sin.) in the Arctic Ocean, *Earth Planet. Sci. Lett.*, *146*(1–2), 47–58.

Bauch, D., and H. A. Bauch (2001), Last glacial benthic foraminiferal d18O anomalies in the polar North Atlantic: A modern analogue evaluation, *J. Geophys. Res.*, *106*(5), 9135–9143.

Bauch, H. A., and M. S. Weinelt (1997), Surface water changes in the Norwegian Sea during last Deglacial and Holocene times, *Quat. Sci. Rev.*, *16*(10), 1115–1124.

Bauch, H. A., H. Erlenkeuser, R. F. Spielhagen, U. Struck, J. Matthiessen, J. Thiede, and J. Heinemeier (2001a), A multiproxy reconstruction of the evolution of deep and surface waters in the subarctic Nordic seas over the last 30,000 yr, *Quat. Sci. Rev.*, *20*(4), 659–678.

Bauch, H. A., T. Mueller-Lupp, E. Taldenkova, R. F. Spielhagen, H. Kassens, P. M. Grootes, J. Thiede, J. Heinemeier, and V. V. Petryashov (2001b), Chronology of the Holocene trangression at the North Siberian margin, *Global Planet. Change 31*, 125–139.

Bianchi, G. G., and I. N. McCave (1999), Holocene periodicity in North Atlantic climate and deep-ocean flow south of Iceland, *Nature*, *397*, 515–517.

Bond, G., W. Showers, M. Cheseby, R. Lotti, P. Almasi, P. deMenocal, P. Priore, H. Cullen, I. Hajdas, and G. Bonani (1997), A pervasive millennial-scale cycle in North Atlantic Holocene and glacial climates, *Science*, *278*, 1257–1266.

Bond, G., B. Kromer, J. Beer, R. Muscheler, M. N. Evans, W. Showers, S. Hoffmann, R. Lotti-Bond, I. Hajdas, and G. Bonani (2001), Persistent solar influence on North Atlantic climate during the Holocene, *Science*, *294*, 2130–2136.

Came, R. E., D. W. Oppo, and J. F. McManus (2007), Amplitude and timing of temperature and salinity variability in the subpolar North Atlantic over the past 10 k.y, *Geology*, *35*(4), 315–318.

Carstens, J., D. Hebbeln, and G. Wefer (1997), Distribution of planktic foraminifera at the ice margin in the Arctic (Fram Strait), *Mar. Micropaleontol.*, *29*(3–4), 257–269.

Chapman, M. R., and N. J. Shackleton (2000), Evidence of 550-year and 1000-year cyclicities in North Atlantic circulation patterns during the Holocene, *Holocene*, *10*(3), 287–291.

Cronin, T. M., L. Gemery, W. M. Briggs, M. Jakobsson, L. Polyak, and E. M. Brouwers (2010), Quaternary Sea-ice history in the Arctic Ocean based on a new Ostracode sea-ice proxy, *Quat. Sci. Rev.*, *29*(25–26), 3415–3429.

Darling, K. F., M. Kucera, D. Kroon, and C. M. Wade (2006), A resolution for the coiling direction paradox in *Neogloboquadrina pachyderma*, *Paleoceanography*, *21*, PA2013, doi:10.1029/2005PA001209.

Denton, G. H., and W. Karlén (1973), Holocene climatic variations: Their pattern and possible cause, *Quat. Res.*, *2*, 155–205.

Dickson, R. R., T.J. Osborn, J.W. Hurrell, J. Meincke, J. Blindheim, B. Adlandsvik, T. Vinje, G. Alekseev, and W. Maslowski (2000), The Arctic Ocean Response to the North Atlantic Oscillation, *J. Clim.*, *13*, 2671–2696.

Duplessy, J. C., E. Ivanova, I. Murdmaa, M. Paterne, and L. Labeyrie (2001), Holocene paleoceanography of the northern Barents Sea and variations of the northward heat transport by the Atlantic Ocean, *Boreas*, *30*(1), 2–16.

Duplessy, J. C., L. Labeyrie, and C. Waelbroeck (2002), Constraints on the ocean oxygen isotopic enrichment between the Last Glacial Maximum and the Holocene: Paleoceanographic implications, *Quat. Sci. Rev.*, *21* (1–3), 315–330.

Dyke, A. S., J. England, E. Reimnitz, and H. Jette (1997), Changes in driftwood delivery to the Canadian arctic archipelago: The hypothesis of postglacial oscillations of the transpolar drift, *Arctic*, *50*(1), 1–16.

Ebbesen, H., M. Hald, and T. H. Eplet (2007), Lateglacial and early Holocene climatic oscillations on the western Svalbard margin, European Arctic, *Quat. Sci. Rev.*, *26*, 1999–2011.

Ellison, C. R., M. R. Chapman, and I. R. Hall (2006), Surface and deep ocean interactions during the cold climate event 8200 years ago, *Science*, *312*(5782), 1929–1932.

Fairbanks, R. G. (1989), A 17,000-year glacio-eustatic sea level record: influence of glacial melting rates on the Younger Dryas event and deep-ocean circulation, *Nature*, *342*, 637–642.

Forwick, M., and T. O. Vorren (2007), Holocene mass-transport activity and climate in outer Isfjorden, Spitsbergen: Marine and subsurface evidence, *Holocene*, *17*(6), 707–716.

Forwick, M., and T. O. Vorren (2009), Late Weichselian and Holocene sedimentary environments and ice rafting in Isfjorden, Spitsbergen, *Palaeogeogr. Palaeoclimatol. Palaeoecol.*, *280*(1–2), 258–274.

Frank, M. (1996), Spurenstoffuntersuchungen zur Zirkulation im Eurasischen Becken des Nordpolarmeeres, PhD thesis, Ruprecht-Karls-Univ., Heidelberg, Germany.

Funder, S., et al. (2011), A 10,000-year record of Arctic Ocean sea-ice variability: View from the beach, *Science*, *333*, 747–750.

Gammelsrød, T., and B. Rudels (1983), Hydrographic and current measurements in the Fram Strait, August 1981, *Polar Res.*, *1*, 115–126.

Gascard, J. C., C. Kergomard, P. F. Jeannin, and M. Fily (1988), Diagnostic study of the Fram Strait marginal ice-zone during summer from 1983 and 1984 marginal ice-zone experiment Langrangian observations, *J. Geophys. Res.*, *93*(C4), 3613–3641.

Hald, M., and R. Aspeli (1997), Rapid climate shifts of the northern Norwegian Sea during the deglaciation and the Holocene, *Boreas*, *26*, 16–28.

Hald, M., H. Ebbesen, M. Forwick, F. Godtliebsen, L. Khomenko, S. Korsun, L. Ringstad Olsen, and T. O. Vorren (2004), Holocene paleoceanography and glacial history of the West Spitsbergen area, Euro-Arctic margin, *Quat. Sci. Rev.*, *23*, 2075–2088.

Hald, M., C. Andersson, H. Ebbesen, E. Jansen, D. Klitgaard Kristensen, B. Risebrobakken, G. R. Salomonsen, M. Sarnthein, H. P. Sejrup, and R. J. Telford (2007), Variations in temperature and extent of Atlantic Water in the northern North Atlantic during the Holocene, *Quat. Sci. Rev.*, *26*, 3423–3440.

Hall, I. R., G. G. Bianchi, and J. R. Evans (2004), Centennial to millennial scale Holocene climate-deep water linkage in the North Atlantic, *Quat. Sci. Rev.*, *23*(14–15), 1529–1536.

Hass, H. C. (2002), A method to reduce the influence of ice-rafted debris on a grain size record from northern Fram Strait, *Polar Res.*, *21*(2), 299–306.

Haugan, P. M. (1999), Structure and heat content of the West Spitsbergen Current, *Polar Res.*, *18*(2), 183–188.

Healy-Williams, N. (1992), Stable Isotope differences among morphotypes of *Neogloboquadrina pachyderma* (Ehrenberg) - Implications for high-latitude paleoceanographic studies, *Terra Nova*, *4*(6), 693–700.

Hebbeln, D. (1991), Spätquartäre Stratigraphie und Paläozeanographie in der Fram-Straße, PhD thesis, 174 pp., Univ. Bremen, Bremen, Germany.

Hopkins, T. S. (1991), The GIN Sea - A synthesis of its physical oceanography and literature review 1972–1985, *Earth Sci. Rev.*, *30*(3–4), 175–318.

Humlum, O., B. Elberling, A. Hormes, K. Fjordheim, O. H. Hansen, and J. Heinemeier (2005), Late-Holocene glacier growth in Svalbard, documented by subglacial relict vegetation and living soil microbes, *Holocene*, *15*(3), 396–407.

Husum, K., and M. Hald (2012), Arctic planktic foraminiferal assemblages: Implications for subsurface temperature reconstructions, *Mar. Micropaleontol.*, *96–97*, 38–47.

Jennings, A. E., K. L. Knudsen, M. Hald, C. V. Hansen, and J. T. Andrews (2002), A mid-Holocene shift in Arctic sea-ice variability on the East Greenland Shelf, *Holocene*, *12*(1), 49–58.

Jennings, A. E., J. Andrews, and L. Wilson (2011), Holocene environmental evolution of the SE Greenland Shelf North and South of the Denmark Strait: Irminger and East Greenland current interactions, *Quat. Sci. Rev.*, *30*(7–8), 980–998.

Jessen, S. P., T. L. Rasmussen, T. Nielsen, and A. Solheim (2010), A new Late Weichselian and Holocene marine chronology for the western Svalbard slope 30,000–0 cal years BP, *Quat. Sci. Rev.*, *29*(9–10), 1301–1312.

Johannessen, O. M. (1986), Brief overview of the physical oceanography, in *The Nordic Seas*, edited by B.G Hurdle, pp. 103–127, Springer, New York.

Johannessen, O. M. (1987), Summer Marginal Ice-Zone Experiments during 1983 and 1984 in Fram Strait and the Greenland Sea - Introduction, *J. Geophys. Res.*, *92*(C7), 6716–6718.

Johannessen, T., E. Jansen, A. Flatøy, and A. C. Ravelo (1994), The relationship between surface water masses, oceanographic fronts and paleoclimatic proxies in surface sediments of the Greenland, Iceland, Norwegian Seas, in *Carbon Cycling in the Glacial Ocean: Constraints of the Ocean's Role in Global Change*, edited by R. Zahn et al., pp. 61–85, Springer, Berlin.

Karcher, M. J., R. Gerdes, F. Kauker, and C. Köberle (2003), Arctic warming: Evolution and spreading of the 1990s warm event in the Nordic seas and the Arctic Ocean, *J. Geophys. Res.*, *108*(C2), 3034, doi:10.1029/2001JC001265.

Kaufman, D. S., D. P. Schneider, N. P. McKay, C. M. Ammann, R. S. Bradley, K. R. Briffa, G. H. Miller, B. L. Otto-Bliesner, J. T. Overpeck, and B. M. Vinther (2009), Recent warming reverses long-term arctic cooling, *Science*, *325*(5945), 1236–1239.

Keigwin, L. D., J.P. Sachs, Y. Rosenthal, and E. A. Boyle (2005), The 8200 year B.P. event in the slope water system, western subpolar North Atlantic, *Paleoceanography*, *20*, PA2003, doi:10.1029/2004PA001074.

Kleiven, H. K., C. Kissel, C. Laj, U. S. Ninnemann, T. O. Richter, and E. Cortijo (2008), Reduced North Atlantic deep water coeval with the glacial Lake Agassiz freshwater outburst, *Science*, *319*(5859), 60–64.

Koç, N., E. Jansen, and H. Haflidason (1993), Paleoceanographic Reconstructions of Surface Ocean Conditions in the Greenland, Iceland and Norwegian Seas through the last 14 ka based on diatoms, *Quat. Sci. Rev.*, *12*, 115–140.

Kozdon, R., A. Eisenhauer, M. Weinelt, M. Y. Meland, and D. Nuernberg (2009), Reassessing Mg/Ca temperature calibrations of *Neogloboquadrina pachyderma* (sinistral) using paired δ44/40Ca and Mg/Ca measurements, *Geochem. Geophys. Geosyst.*, *10*, Q03005, doi:10.1029/2008GC002169.

Kucera, M., et al. (2005), Reconstruction of sea-surface temperatures from assemblages of planktonic foraminifera: Multi-technique approach based on geographically constrained calibration data sets and its application to glacial Atlantic and Pacific Oceans, *Quat. Sci. Rev.*, *24*(7–9), 951–998.

Laskar, J., P. Robutel, F. Joutel, M. Gastineau, A. C. M. Correia, and B. Levrard (2004), A long-term numerical solution for the insolation quantities of the Earth, *Astron. Phys.*, *428*(1), 261–285.

Lubinski, D. J., L. Polyak, and S. L. Forman (2001), Freshwater and Atlantic water inflows to the deep northern Barents and Kara seas since ca 13 14C ka: foraminifera and stable isotopes, *Quat. Sci. Rev.*, *20*(18), 1851–1879.

Manabe, S., and R. J. Stouffer (1980), Sensitivity of a global climate model to an increase of CO_2 concentration in the atmosphere, *J. Geophys. Res.*, *85*(C10), 5529–5554.

Mann, M. E., Z. Zhang, S. Rutherford, R. S. Bradley, M. K. Hughes, D. Shindell, C. Ammann, G. Faluvegi, and F. Ni (2009), Global signatures and dynamical origins of the Little Ice Age and Medieval Climate Anomaly, *Science*, *326*(5957), 1256–1260.

Marnela, M., B. Rudels, K. A. Olsson, L. G. Anderson, E. Jeansson, D. J. Torres, M. J. Messias, J. H. Swift, and A. J. Watson (2008), Transports of Nordic Seas water masses and excess SF(6) through Fram Strait to the Arctic Ocean, *Prog. Oceanogr.*, *78*(1), 1–11.

McDermott, F., et al. (1999), Holocene climate variability in Europe: Evidence from δO18, textural and extension-rate variations in three speleothems, *Quat. Sci. Rev.*, *18*(8–9), 1021–1038.

Meredith, M., K. Heywood, P. Dennis, L. Goldson, R. White, E. Fahrbach, U. Schauer, and S. Østerhus (2001), Freshwater fluxes through the Western Fram Strait, *Geophys. Res. Lett.*, *28*(8), 1615–1618.

Moberg, A., D. M. Sonechkin, K. Holmgren, N. M. Datsenko, and W. Karlén (2005), Highly variable Northern Hemisphere temperatures reconstructed from low- and high-resolution proxy data, *Nature*, *433*, 613–617.

Moritz, R. E., C. M. Bitz, and E. J. Steig (2002), Dyamics of recent climate change in the Arctic, *Science*, *297*, 1497–1502.

Moros, M., K. Emeis, B. Risebrobakken, I. Snowball, A. Kuijpers, J. McManus, and E. Jansen (2004), Sea surface temperatures and ice rafting in the Holocene North Atlantic: Climate influences on Northern Europe and Greenland, *Quat. Sci. Rev.*, *23*(20–22), 2113–2126.

Moros, M., J. T. Andrews, D. D. Eberl, and E. Jansen (2006), Holocene history of drift ice in the northern North Atlantic: Evidence for different spatial and temporal modes, *Paleoceanography*, *21*, PA2017, doi:10.1029/2005PA001214.

Müller, J., K. Werner, R. Stein, K. Fahl, M. Moros, and E. Jansen (2012), Holocene cooling culminates in Neoglacial sea ice oscillations in Fram Strait, *Quat. Sci. Rev.*, *47*, 1–14.

Nesje, A., and M. Kvamme (1991), Holocene glacier and climate variations in western Norway - Evidence for early Holocene glacier demise and multipe neoglacial events, *Geology*, *19*(6), 610–612.

Overpeck, J., et al. (1997), Arctic environmental change of the last four centuries, *Science*, *278*(5341), 1251–1256.

Pflaumann, U., J. Duprat, C. Pujol, and L. D. Labeyrie (1996), SIMMAX: A modern analog technique to deduce Atlantic sea surface temperatures from planktonic foraminifera in deep-sea sediments, *Paleoceanography*, *11*(1), 15–35.

Pflaumann, U., et al. (2003), Glacial North Atlantic: Sea surface conditions reconstructed by GLAMAP 2000, *Paleoceanography*, *18*(3), 1065, doi:10.1029/2002PA000774.

Prange, M., and G. Lohmann (2003), Effects of mid-Holocene river runoff on the Arctic ocean/sea-ice system: A numerical model study, *Holocene*, *13*(3), 335–342.

Quadfasel, D., B. Rudels, and K. Kurz (1988), Outflow of dense water from a Svalbard fjord into the Fram Strait, *Deep Sea Res., Part A*, *35*(7), 1143–1150.

Rabe, B., U. Schauer, A. Mackensen, M. Karcher, E. Hansen, and A. Beszczynska-Moller (2009), Freshwater components and transports in the Fram Strait - recent observations and changes since the late 1990s, *Ocean Sci.*, *5*(3), 219–233.

Rasmussen, S. O., et al. (2006), A new Greenland ice core chronology for the last glacial termination, *J. Geophys. Res.*, *111*, D06102, doi:10.1029/2005JD006079.

Rasmussen, T. L., and E. Thomsen (2009), Stable isotope signals from brines in the Barents Sea: Implications for brine formation during the last glaciation, *Geology*, *37*(10), 903–906.

Rasmussen, T. L., E. Thomsen, M. A. Slubowska, S. Jessen, A. Solheim, and N. Koc (2007), Paleoceanographic evolution of the SW Svalbard margin (76¬∞N) since 20,000 14C yr BP, *Quat. Res.*, *67*(1), 100–114.

Rasmussen, T. L., M. Forwick, and A. Mackensen (2012), Reconstruction of inflow of Atlantic Water to Isfjorden, Svalbard during the Holocene: Correlation to climate and seasonality, *Mar. Micropaleontol.*, *94–95*, 80–90.

Renssen, H., H. Goosse, and T. Fichefet (2002), Modeling the effect of freshwater pulses on the early Holocene climate: The influence of high-frequency climate variability, *Paleoceanography*, *17*(2), 1020, doi:10.1029/2001PA000649.

Risebrobakken, B., E. Jansen, C. Andersson, E. Mjelde, and K. Hevrøy (2003), A high-resolution study of Holocene paleoclimatic and paleoceanographic changes in the Nordic Seas, *Paleoceanography*, *18*, PA1017, doi:10.1029/2002PA000764

Risebrobakken, B., M. Moros, E. V. Ivanova, N. Chistyakova, and R. Rosenberg (2010), Climate and oceanographic variability in the SW Barents Sea during the Holocene, *Holocene*, *20*(4), 609–621.

Risebrobakken, B., T. Dokken, L. H. Smedsrud, C. Andersson, E. Jansen, M. Moros, and E. Ivanova (2011), Early Holocene temperature variability in the Nordic Seas: The role of oceanic heat advection versus changes in orbital forcing, *Paleoceanography*, *26*, PA4206, doi:10.1029/2011PA002117.

Robinson, S. G., and I. N. McCave (1994), Orbital forcing of bottom-current enhanced sedimentation on Feni Drift, NE Atlantic, during the Mid-Pleistocene, *Paleoceanography*, *9*(6), 943–972.

Rohling, E. J., and H. Pälike (2005), Centennial-scale climate cooling with a sudden cold event around 8,200 years ago, *Nature*, *434*, 975–979.

Rudels, B., G. Bjork, J. Nilsson, P. Winsor, I. Lake, and C. Nohr (2005), The interaction between waters from the Arctic Ocean and the Nordic Seas north of Fram Strait and along the East Greenland Current: Results from the Arctic Ocean-02 Oden expedition, *J. Mar. Syst.*, *55*(1–2), 1–30.

Saloranta, T. M., and P. M. Haugan (2004), Northward cooling and freshening of the warm core of the West Spitsbergen Current, *Polar Res.*, *23*(1), 447–461.

Sarnthein, M., S. van Kreveld, H. Erlenkeuser, P. M. Grootes, M. Kucera, U. Pflaumann, and M. Schulz (2003), Centennial-to-millennial-scale periodicities of Holocene climate and sediment injections off the western Barents shelf, 75°N, *Boreas*, *32*, 447–461.

Schauer, U. (1989), Hydrographie der Fram Straße, report, Inst. für Meereskunde, Hamburg, Germany.

Schauer, U. (1995), The release of brine-enriched shelf water from Storfjord into the Norwegian Sea, *J. Geophys. Res.*, *100*(C8), 16,015–16,028.

Schauer, U., E. Fahrbach, S. Osterhus, and G. Rohardt (2004), Arctic warming through the Fram Strait: Oceanic heat transport from 3 years of measurements, *J. Geophys. Res.*, *109*, C06026, doi:10.1029/2003JC001823.

Schlichtholz, P., and M.-N. Houssais (1999), An inverse modeling study in Fram Strait. Part II: Water mass distribution and transports, *Deep Sea Res. Part II*, *46*(6–7), 1137–1168.

Schmidt, G. A., G. R. Bigg, and E. J. Rohling (1999), Global Seawater Oxygen-18 Database, edited, http://data.giss.nasa.gov/o18data/.

Schulz, M., and A. Paul (2002), Holocene Climate Variability on Centennial-to-Millennial Time Scales: 1. Climate Records from the North Atlantic Realm, in *Climate Development and History of the North Atlantic Realm*, edited by G. Wefer and et al., pp. 41–54, Springer, Berlin.

Schulz, M., A. Paul, and A. Timmermann (2004), Glacial-interglacial contrast in climate variability at centennial-to-millennial timescales: Observations and conceptual model, *Quat. Sci. Rev.*, *23*(20–22), 2219–2230.

Seidenkrantz, M.-S., L. Roncaglia, A. Fischel, C. Heilmann-Clausen, A. Kuijpers, and M. Moros (2008), Variable North Atlantic climate seesaw patterns documented by a late Holocene marine record from Disko Bugt, West Greenland, *Mar. Micropaleontol.*, *68*(1–2), 66–83.

Seppä, H., and H. J. B. Birks (2001), July mean temperature and annual precipitation trends during the Holocene in the Fennoscandian tree-line area: pollen-based climate reconstructions, *Holocene 11*, 527–539.

Serreze, M. C., and J. A. Francis (2006), The Arctic amplification debate, *Clim. Change*, *76*, 241–264.

Serreze, M. C., M. M. Holland, and J. Stroeve (2007), Perspectives on the Arctic's shrinking sea-ice cover, *Science*, *315*(5818), 1533–1536.

Shackleton, N. J., and N. D. Opdyke (1973), Oxygen isotope and palaeomagnetic stratigraphy of equatorial Pacific Core V28-238: Oxygen isotope temperatures and ice volumes on a 105 year and 106 year scale, *Quat. Res. 3*, 39–55.

Simstich, J., M. Sarnthein, and H. Erlenkeuser (2003), Paired δ18O signals of *Neogloboquadrina pachyderma* (s) and *Turborotalita quinqueloba* show thermal stratification structure in Nordic Seas, *Mar. Micropaleontol.*, *48*(1–2), 107–125.

Ślubowska, M. A., N. Koç, T. L. Rasmussen, and D. Klitgaard Kristensen (2005), Changes in the flow of Atlantic water into the Arctic Ocean since the last deglaciation: Evidence from the northern Svalbard continental margin, 80°N, *Paleoceanography*, *20*, PA4014, doi:10.1029/2005PA001141.

Ślubowska-Woldengen, M., T. L. Rasmussen, N. Koç, D. Klitgaard-Kristensen, F. Nilsen, and A. Solheim (2007), Advection of Atlantic Water to the western and northern Svalbard shelf since 17,500 cal yr BP, *Quat. Sci. Rev.*, *26*(3–4), 463–478.

Ślubowska-Woldengen, M., N. Koç, T. L. Rasmussen, D. Klitgaard-Kristensen, M. Hald, and A. E. Jennings (2008), Time-slice reconstructions of ocean circulation changes on the continental shelf in the Nordic and Barents Seas during the last 16,000 cal yr B.P, *Quat. Sci. Rev.*, *27* (15–16), 1476–1492.

Spielhagen, R. F., and H. Erlenkeuser (1994), Stable oxygen and carbon isotopes in planktic foraminifers from the Arctic Ocean surface sediments: Reflection of the low salinity surface water layer, *Mar. Geol. 119*, 227–250.

Spielhagen, R. F., K. Werner, S. A. Sorensen, K. Zamelczyk, E. Kandiano, G. Budeus, K. Husum, T. M. Marchitto, and M. Hald (2011), Enhanced modern heat transfer to the Arctic by warm Atlantic Water, *Science*, *331*(6016), 450–453.

Stuiver, M., P. M. Grootes, and T. F. Braziunas (1995), The GISP2 d18O climate record of the past 16,500 years and the role of the Sun, ocean, and volcanoes, *Quat. Res.*, *44*, 341–354.

Svendsen, J. I., and J. Mangerud (1997), Holocene glacial and climatic variations on Spitsbergen, Svalbard, *The Holocene*, *7*(1), 45–57.

Vinje, T. (2001), Anomalies and trends of sea-ice extent and atmospheric circulation in the Nordic Seas during the period 1864–1998, *J. Clim.*, *14*(3), 255–267.

Vinther, B. M., et al. (2006), A synchronized dating of three Greenland ice cores throughout the Holocene, *J. Geophys. Res.*, *111*, D15107, doi:10.1029/2005JD006921.

Volkmann, R. (2000), Planktic foraminifer ecology and stable isotope geochemistry in the Arctic Ocean: Implications from water column and sediment surface studies for quantitative reconstructions of oceanic Parameters, *Ber. Polarforsch.*, *361*, 1–128.

Wanner, H., et al. (2008), Mid- to Late Holocene climate change: An overview, *Quat. Sci. Rev.*, *27*(19–20), 1791–1828.

Wanner, H., O. Solomina, M. Grosjean, S. P. Ritz, and M. Jetel (2011), Structure and origin of Holocene cold events, *Quat. Sci. Rev.*, *30*(21–22), 3109–3123.

Werner, K., R. F. Spielhagen, D. Bauch, H. C. Hass, E. Kandiano, and K. Zamelczyk (2011), Atlantic Water advection to the eastern Fram Strait — Multiproxy evidence for late Holocene variability, *Palaeogeogr. Palaeoclimatol. Palaeoecol.*, *308*(3–4), 264–276.

Williams, K. M. (1993), Ice-sheet and ocean interactions, margin of the east Greenland ice-sheet (14 ka to present): Diatom evidence, *Paleoceanography*, *8*(1), 69–83.